

①

Multilayer relaxation of the Fe{210} surface

J. Sokolov* and F. Jona

Department of Materials Science and Engineering, State University of New York, Stony Brook, New York 11794

P. M. Marcus

IBM Thomas J. Watson Research Center, PO Box 218, Yorktown Heights, New York 10598

(Received 3 August 1984)

The surface structure of body-centered-cubic Fe{210} has been determined by low-energy-electron-diffraction intensity analysis. Substantial relaxations from bulklike structure in directions both perpendicular and parallel to the surface were found. The {210} surface is the most open of the six Fe surfaces that have been studied, shows the largest perpendicular relaxation, involves the most structural parameters (8), and has been determined to the greatest depth (down to the fifth layer). The observed structure is as follows: spacing between first and second layer $d_{12}=0.50\pm 0.03 \text{ \AA}$ (bulk spacing is 0.641 \AA), in similar notation $d_{23}=0.57\pm 0.03 \text{ \AA}$, $d_{34}=0.75\pm 0.03 \text{ \AA}$, $d_{45}=0.61\pm 0.03 \text{ \AA}$; change of registry shift between first and second layer $\Delta a_{12}=0.14\pm 0.05 \text{ \AA}$, in similar notation $\Delta a_{23}=0.03\pm 0.05 \text{ \AA}$, $\Delta a_{34}=0.00\pm 0.05 \text{ \AA}$, $\Delta a_{45}=0.08\pm 0.05 \text{ \AA}$.

DTIC ELECTE
NOV 01 1988
S E

AD-A201 501

I. INTRODUCTION

Much recent work by low-energy-electron diffraction (LEED) intensity analysis has established accurately and reliably the relaxations of the surface layers of a number of clean metal surfaces, where the term relaxation refers to rigid translations of the surface layers from their bulk positions without change of the unit cell of the surface mesh. Our work on higher index, less symmetrical, more open surfaces of bcc iron, i.e., Fe{211}, Fe{310}, and Fe{210}, has demonstrated the occurrence of parallel as well as perpendicular relaxations, both of which have damped oscillatory magnitudes, extend deep into the surface, and increase in magnitude with surface openness or roughness. Iron, reprints. (Sign)

The present work gives details of the analysis of the Fe{210} surface, which is the most open of the six surfaces of Fe that have been studied, involves the largest number of structural parameters, and is found to have the largest perpendicular relaxation (22% contraction) of any of these surfaces. This large perpendicular relaxation is in qualitative agreement with the idea of a relaxation driven by a surface Madelung force arising from the flattening of the electron density at the surface, hence a Madelung force which is larger for more open surfaces.⁶ The Madelung force model has been developed⁷ by making simple assumptions about the electron density and the electron response and then allowing the lattice to relax so as to minimize the total energy. These models have led to interesting qualitative features of the relaxation to compare with measured relaxations, as will be noted later. However deduction of the ground state from first principles by relaxation to self-consistency of both the electron density and the nuclear positions has not yet been achieved, even for a simple metal; a transition metal like Fe would be still more difficult. Hence the results found

here provide valuable information for further development of the fundamental theory of metal surfaces. In addition, we note that structural changes of the magnitude found here can no longer be regarded as small and it is clearly necessary to fix the atom positions in the surface layers before quantitative theories of surface properties, e.g., vibrational models and electronic states, are possible.

The Fe{210} surface was found to have relaxation effects down to at least the fifth layer including displacements both parallel and perpendicular to the surface. Section II gives experimental details; Secs. III and IV describe the calculations and structure analysis, respectively.

II. EXPERIMENTAL

The methods for preparing an oriented single-crystal Fe{210} sample and the procedure for cleaning the crystal *in vacuo* were the same as for Fe{310}.⁵ Thirty-five LEED intensity-versus-energy spectra (31 nondegenerate) were collected with a spot photometer: sixteen spectra at normal incidence ($0\bar{1}$, 10 , 11 , $1\bar{1}$, 10 , 20 , $1\bar{1}$, $1\bar{1}$, 20 , 30 , $2\bar{1}$, 21 , $0\bar{2}$, 30 , $2\bar{1}$, and $2\bar{1}$), ten spectra at $\theta=7.4^\circ, \phi=90^\circ$ (00 , 10 , 10 , 11 , 11 , $1\bar{1}$, $2\bar{1}$, 21 , 20 , and 30) and nine spectra at $\theta=13.2^\circ, \phi=90^\circ$ (00 , 10 , 20 , 30 , $3\bar{1}$, $1\bar{2}$, 21 , $1\bar{1}$, and $3\bar{2}$). All data were collected with the crystal at room temperature and the angles and beam indices follow the convention of Zanazzi *et al.*⁸ A schematic drawing of the LEED pattern is shown in Fig. 1.

III. CALCULATIONS

LEED intensity spectra were calculated with the computer program CHANGE.^{9,10} The very small interlayer spacing of Fe{210} ($d_{\text{bulk}}=0.641 \text{ \AA}$) and the correspondingly large surface unit cell ($2.87 \text{ \AA} \times 6.41 \text{ \AA}$) necessitated

①

9 2 1 0 3 1 2 2 8

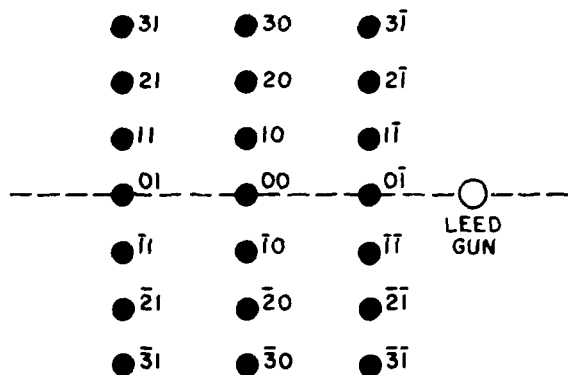


FIG. 1. Schematic LEED pattern of Fe{210} for $\theta=0^\circ$, $\phi=90^\circ$.

the use of up to 123 plane waves, or beams, to represent the wave function accurately for calculating interlayer scattering. Up to five planes of atoms were bunched together into composite layers, among which the scattering was calculated in the spherical wave basis, rather than the beam basis, and hence was not restricted to widely spaced layers. The Fe potential was the same as used for previous iron work.¹¹ Eight phase shifts were used to represent ion core scattering and the mean vibrational amplitude was taken as $\langle u^2 \rangle^{1/2} = 0.115 \text{ \AA}$. The complex inner potential $V_i = V_0 - i\beta$ was taken as energy independent, β was set up to 4 eV, and V_0 was left to be determined from the intensity analysis with the initial value fixed at -11.5 eV .

TABLE I. Surface lattice vector \mathbf{a}_1 , and \mathbf{a}_2 , parallel component c_{par} of the interlayer translation vector, interlayer distance d , and mirror plane m for the bulklike Fe{210} surface. \hat{x} and \hat{y} are directed along $\langle 210 \rangle$ and $\langle 100 \rangle$, respectively, as labeled in the top view of Fig. 2; \hat{z} is directed along the inward surface normal. $a = 2.866 \text{ \AA}$.

\mathbf{a}_1	$\sqrt{5}a\hat{x}$
\mathbf{a}_2	$a\hat{y}$
c_{par}	$3a\hat{x}\sqrt{5}/10 + a\hat{y}/2$
d	$a/2\sqrt{5}$
m	$\{100\}$

IV. STRUCTURE ANALYSIS

The bulklike Fe{210} surface is stepped and consists of $\{110\}$ terraces four atomic rows wide joined by monatomic $\{110\}$ steps. Top- and side-view diagrams of the surface are shown in Fig. 2; Table I gives the structural parameters. The unit cell is a rectangle with lattice vectors \mathbf{a}_1 directed along a $\langle 210 \rangle$ axis and of length 6.41 \AA and \mathbf{a}_2 along a $\langle 100 \rangle$ axis and of length 2.87 \AA . The interlayer translation vector \mathbf{c} is in a (closed-packed) $\langle 111 \rangle$ direction with $|\mathbf{c}| = 2.48 \text{ \AA}$. The interlayer spacing is 0.641 \AA and the bulklike registry of successive layers is described by the relation: $c_{\text{par}} = 3\mathbf{a}_1/10 + \mathbf{a}_2/2$, where c_{par} is the projection of \mathbf{c} onto the $\{210\}$ plane. The surface is very open, with a packing fraction of 0.2634 (the most

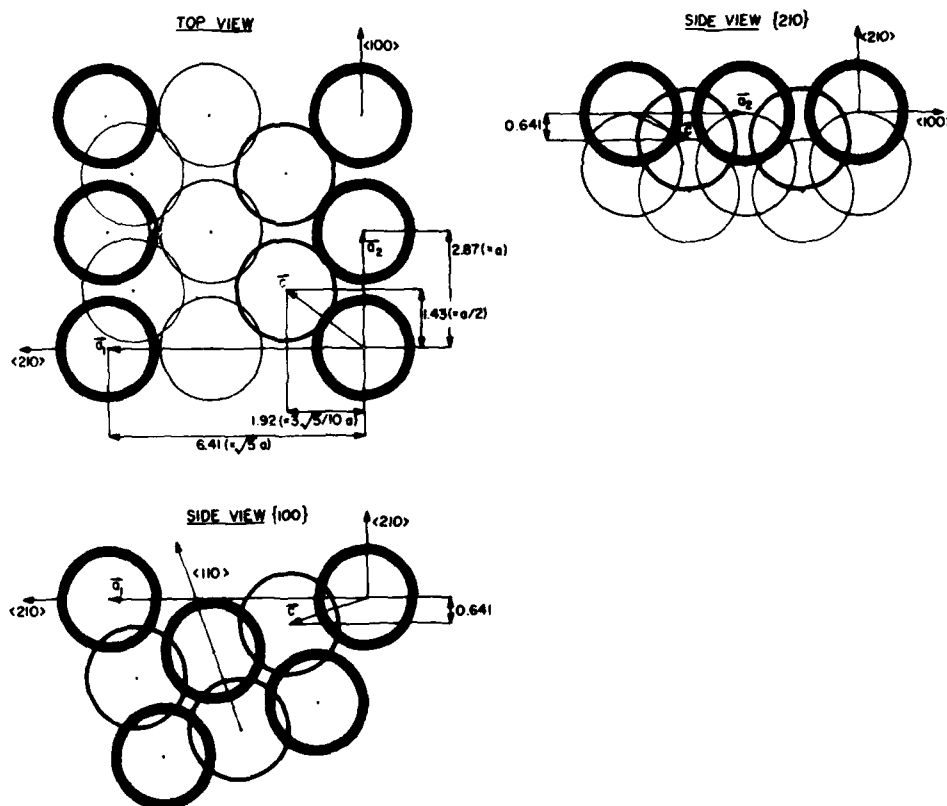


FIG. 2. Top and side views of the undistorted Fe{210} surface. Circles of equal thickness represent coplanar atoms, for the top view circles of decreasing thickness indicate progressively deeper layers. All distances are in \AA .

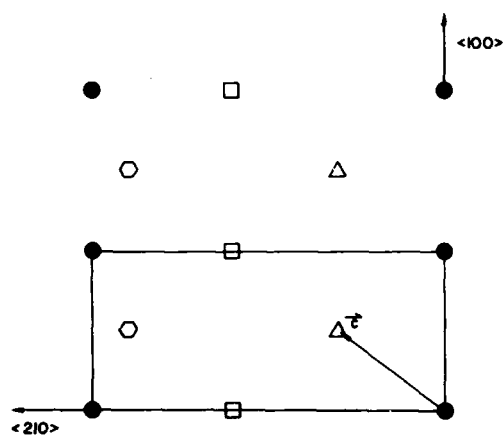


FIG. 3. Schematic of the top four layers of the Fe{210} surface. Circles, first layer; triangles, second layer; squares, third layer; hexagons, fourth layer.

densely packed bcc surface, {110}, has a packing fraction of 0.8330). Six layers are visible at the surface in a touching hard-sphere model and fourth-layer atoms are at a nearest-neighbor distance (2.48 Å) from their closest neighbors in the top layer (see Fig. 3). Hence, there are many nonequivalent atoms which can be legitimately described as surface atoms, a fact which makes the {210} face both interesting and complex. For example, numerous different adsorption sites exist on the surface for chemisorbed monolayers. We have performed experi-

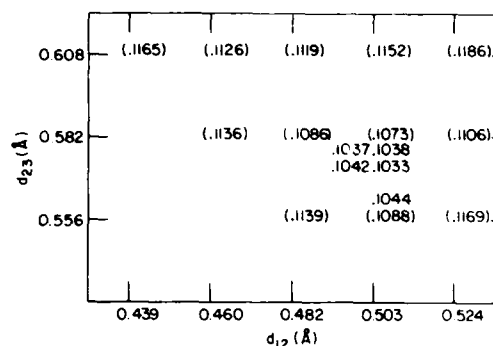


FIG. 4. Variation of the r factor for the $\theta=0^\circ$ data set as a function of d_{12} and d_{23} with $d_{34}=0.748$ Å (0.735 Å), $d_{45}=0.606$ Å (0.621 Å), $a_{12}=2.056$ Å, $a_{23}=1.958$ Å (1.921 Å), $a_{34}=1.942$ Å (1.979 Å), $a_{45}=1.995$ Å, and $V_0=-11.5$ eV.

ments studying oxygen and sulfur structures. Both oxygen and sulfur form (2×1) overlayers but as yet the structures of these systems remain unsolved.

The structural models considered included variations of the first four interlayer spacings, d_{12} , d_{23} , d_{34} , and d_{45} ($d_{\text{bulk}}=0.641$ Å), and the first four registry shifts, a_{12} , a_{23} , a_{34} , and a_{45} (the registry shift between successive layers i and j is defined by $c_{\text{par},ij}=a_2/2+a_{ij}\hat{x}$, the bulk value of a_{ij} is 1.923 Å).

The first series of calculations involved independent variations of the first three interlayer spacings and the top-layer registry, by relatively large amounts, in order to

TABLE II. Results of calculations for $\theta=0^\circ$ of various structural models: d_{12} , d_{23} , and d_{34} are the first three interlayer spacings, a_{12} and a_{23} are the first two interlayer registry parameters (see text). The agreement between theory experiment is given by the reliability factor r . All distances are in Å.

Run	d_{12}	d_{23}	d_{34}	a_{12}	a_{23}	a_{34}	r
1(bulk)	0.641	0.641	0.641	1.923	1.923	1.923	0.293
2	0.561	0.641	0.641	2.188	1.923	1.923	0.216
3	0.587	0.614	0.641	2.320	1.923	1.923	0.236
4	0.561	0.614	0.641	2.452	1.923	1.923	0.249
5	0.561	0.667	0.641	2.188	1.923	1.923	0.226
6	0.561	0.640	0.667	2.320	1.923	1.923	0.235
7	0.534	0.587	0.641	2.188	1.923	1.923	0.208
8	0.534	0.587	0.641	2.055	1.923	1.923	0.185
9	0.561	0.587	0.641	2.055	1.923	1.923	0.194
10	0.561	0.693	0.641	2.188	1.923	1.923	0.270
11	0.534	0.640	0.641	2.188	1.923	1.923	0.187
12	0.534	0.693	0.641	2.188	1.923	1.923	0.270
13	0.540	0.667	0.640	2.188	1.923	1.923	0.179
14	0.518	0.667	0.640	2.188	1.923	1.923	0.164
15	0.518	0.614	0.640	2.188	1.923	1.923	0.154
16	0.518	0.614	0.667	2.188	1.923	1.923	0.144
17	0.518	0.598	0.693	2.188	1.923	1.923	0.142
18	0.508	0.598	0.693	2.108	1.923	1.923	0.138
19	0.497	0.598	0.693	2.108	1.923	1.923	0.132
20	0.503	0.598	0.730	2.108	1.923	1.923	0.127
21	0.503	0.598	0.730	2.108	1.976	1.923	0.127
22	0.503	0.598	0.730	2.108	2.029	1.923	0.128
23	0.503	0.598	0.704	2.055	1.997	1.923	0.124
24	0.496	0.581	0.708	2.056	1.995	1.923	0.118
25	0.496	0.581	0.708	2.056	1.995	1.976	0.115

TABLE III. r factors for the bulklike and fully relaxed models for data collected at three angles of incidence.

Data set	r factors		Energy range (eV)
	Bulklike	Relaxed	
$\theta=0^\circ$	0.293	0.103	1958
$\theta=7.4^\circ$ $\phi=90^\circ$	0.207	0.113	928
$\theta=13.2^\circ$ $\phi=90^\circ$	0.347	0.125	716
Total	0.282	0.110	3602

get a general idea of what the optimum structure might be. Agreement between theory and experimental spectra was measured using the numerical reliability factor of Zanazzi and Jona.¹² For each calculation, the value of the nonstructural parameter V_0 , the real part of the inner potential, was allowed to vary independently from -7.5 to -15.5 eV; the best value was always close to -11.5 eV. A sampling of the first set of calculations (about $\frac{1}{3}$ of the total number of calculations) is shown in Table II labeled with run numbers 1–20. Next, preliminary calculations were made varying the second and third registry shifts, a_{23} and a_{34} (runs 21–25 of Table II are a sampling). At this stage, the calculations indicated that the best models were those with d_{12} contracted ($\approx 20\%$), d_{23} contracted ($\approx 10\%$), d_{34} increased ($\approx 11\%$), a_{12} , a_{23} , and a_{34} increased by approximately 7%, 4%, and 3%, respectively, compared to the bulk values. The next series of calculations fixed all but two of the structural parameters (set near to the corresponding values found above) and then allowed the remaining two parameters to vary independently until a two-dimensional minimum of the reliability factor was located. The best values of the two variables were determined by fitting the r (reliability) factors to a quadratic function (elliptic paraboloid) near the minimum. With the best values thus obtained, a new pair of variables was chosen and the process repeated. Overlapping of pairs was considered, for example (d_{12}, d_{23}), (d_{34}, d_{45}), and (d_{23}, d_{34}); when the consistency among optimum values determined as members of different pairs was as good or better than the estimated experimental un-

certainties (for a discussion of uncertainties in LEED, see Sokolov *et al.*⁴), the analysis was considered finished. An example of the sensitivity of the r factor to the parameter values is given in Fig. 4 for the pair (d_{12}, d_{23}). For the variables whose best values were determined as members of different pairs (a_{23} , a_{34} , d_{23} , and d_{34}) an average of the two "best" values was taken for the final results quoted below. In all cases, the difference between the two best values were 0.01 Å or less. The results of the analysis (with estimated errors following Sokolov *et al.*⁴) were as follows: (bulk interlayer spacing 0.641 Å, bulk layer-to-layer registry shift 1.923 Å)

$$d_{12} = 0.50 \pm 0.03 \text{ \AA} \quad (22.0 \pm 4.7\% \text{ contraction}),$$

$$d_{23} = 0.57 \pm 0.03 \text{ \AA} \quad (11.1 \pm 4.7\% \text{ contraction}),$$

$$d_{34} = 0.75 \pm 0.03 \text{ \AA} \quad (17.0 \pm 4.7\% \text{ expansion}),$$

$$d_{45} = 0.61 \pm 0.03 \text{ \AA} \quad (4.8 \pm 4.7\% \text{ expansion}),$$

$$a_{12} = 2.06 \pm 0.05 \text{ \AA} \quad (7.1 \pm 1.6\% \text{ increase}),$$

$$a_{23} = 1.95 \pm 0.05 \text{ \AA} \quad (1.4 \pm 2.6\% \text{ increase}),$$

$$a_{34} = 1.92 \pm 0.05 \text{ \AA} \quad (0 \pm 2.6\%),$$

$$a_{45} = 2.00 \pm 0.05 \text{ \AA} \quad (4.0 \pm 2.6\% \text{ increase}),$$

$$V_0 = -11.5 \pm 1.0 \text{ eV},$$

$$r_{\min} = 0.103 \quad (r \text{ factor of Zanazzi and Jona}^{12} \text{ for 16 beams at } \theta=0^\circ).$$

The percentage changes are with respect to the bulk values. Figure 5 shows a schematic representation of the optimized structure.

Calculations were then made with the above optimum values for the data sets taken at off-normal incidence. Because of the extreme length of the calculations (about 4 h of CPU time on an IBM 3081 computer), it was not possible to repeat the $\theta=0^\circ$ analysis for the other data sets. Table III gives the r factors for both the bulklike and fully relaxed models for all 35 I -vs- V spectra and Figs. 6–8 show the plots of the corresponding curves.

It should be emphasized at this point that this structural problem, involving eight structural parameters, is notably more difficult than any other attempted so far for metal surfaces. Thus, the optimization process carried out in this work is not exhaustive, and further refinement would be expected to improve the agreement between theory and experiment (particularly for spectra like the $\bar{2}\bar{1}$ beam at $\theta=0^\circ$ and the $\bar{3}0$ beam at $\theta=7.4^\circ$, $\phi=90^\circ$).

To summarize, the loosely packed Fe{210} surface was found to have large relaxations, both normal and parallel to the surface plane. The pattern of contraction, contraction, expansion, and contraction for d_{12} , d_{23} , d_{34} , and d_{45} , respectively, is in agreement with the form predicted for bcc Na{210}.⁷ However, our results for the parallel relaxations (all parallel motions in the same direction) do not agree with the results of Barnett *et al.*⁷ The calculations did not include the effects of screening of the ions by valence electrons and so it is an open question as to whether a more refined theory would give results closer to the observed Fe{210} structure or differences between the

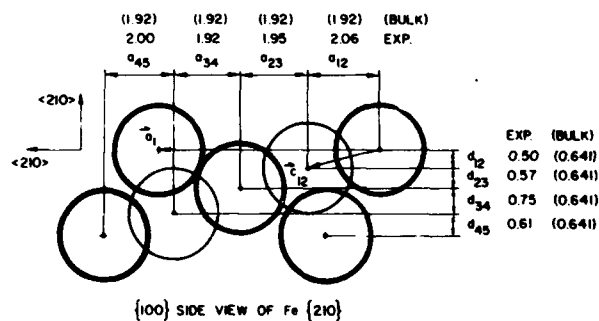


FIG. 5. Schematic of relaxed Fe{210} surface with optimized structural parameters. All distances are in Å.

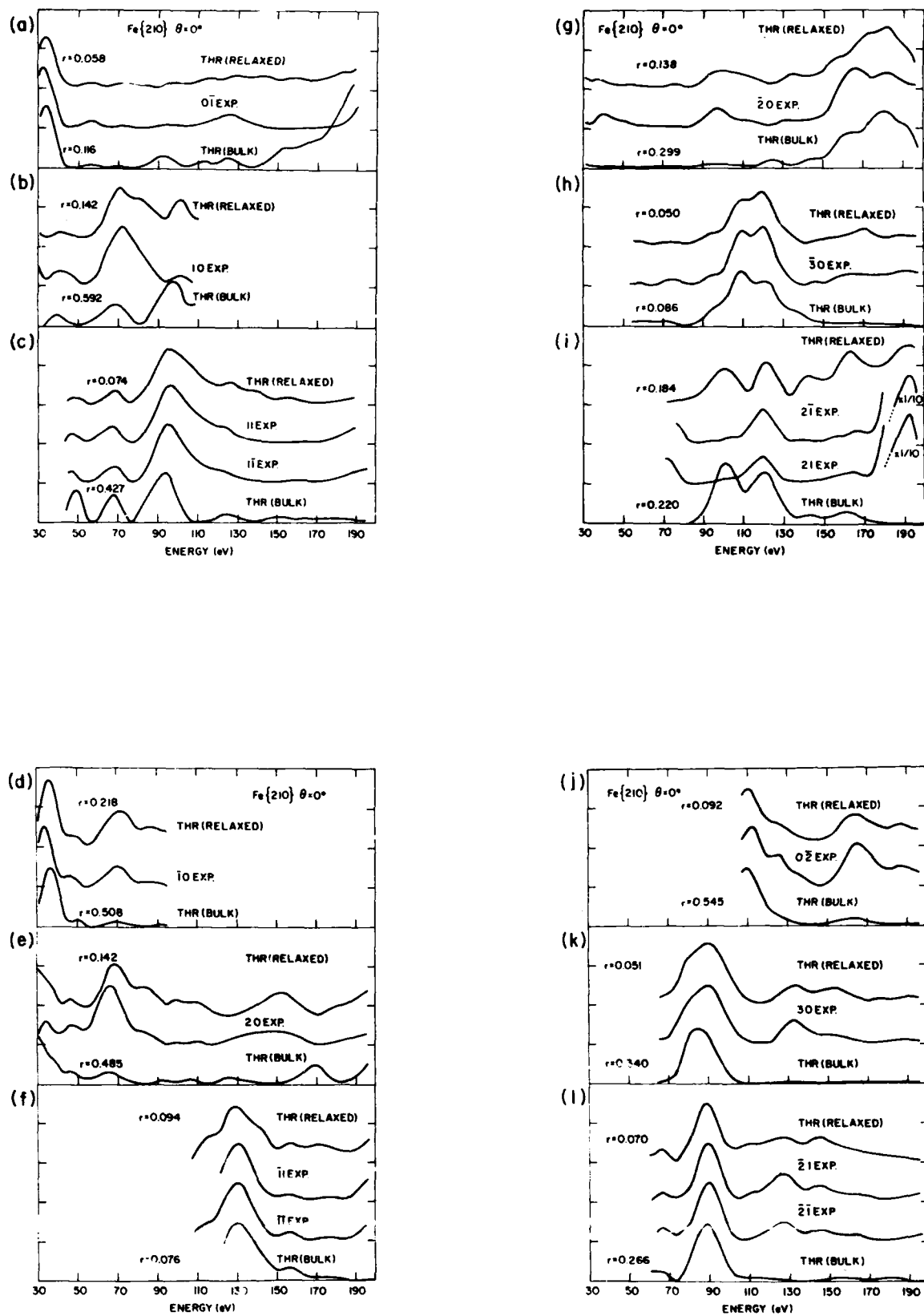
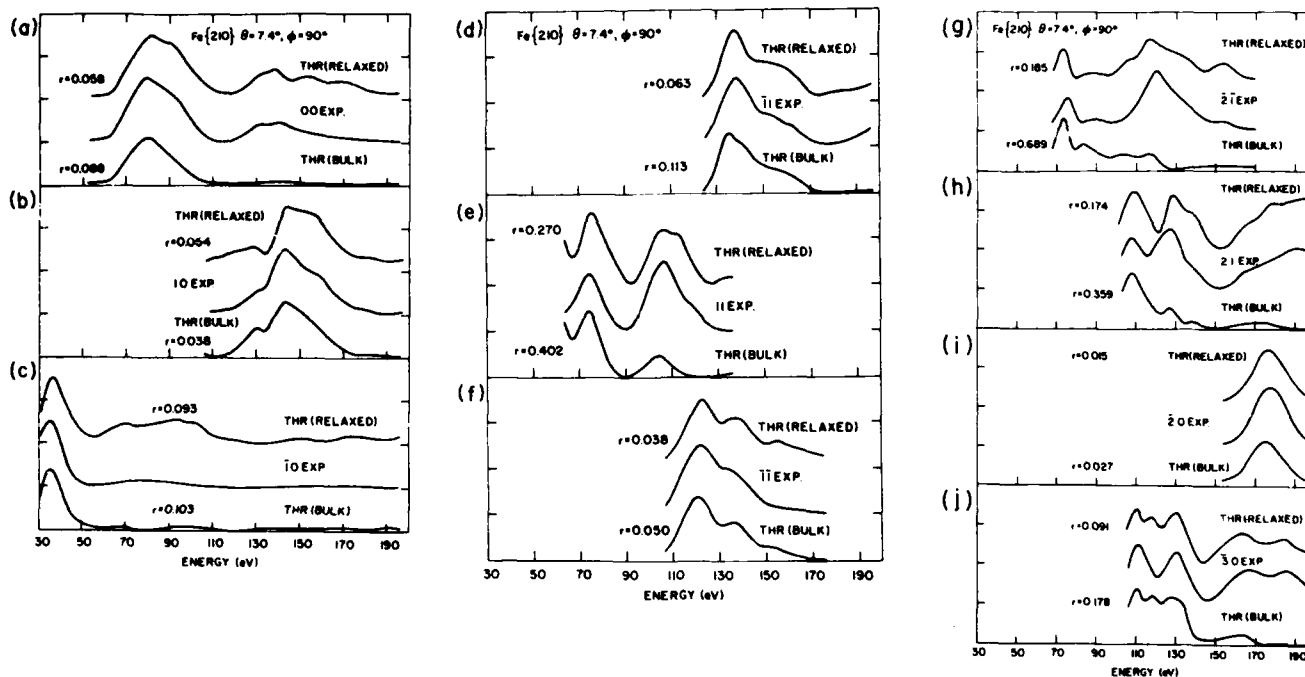
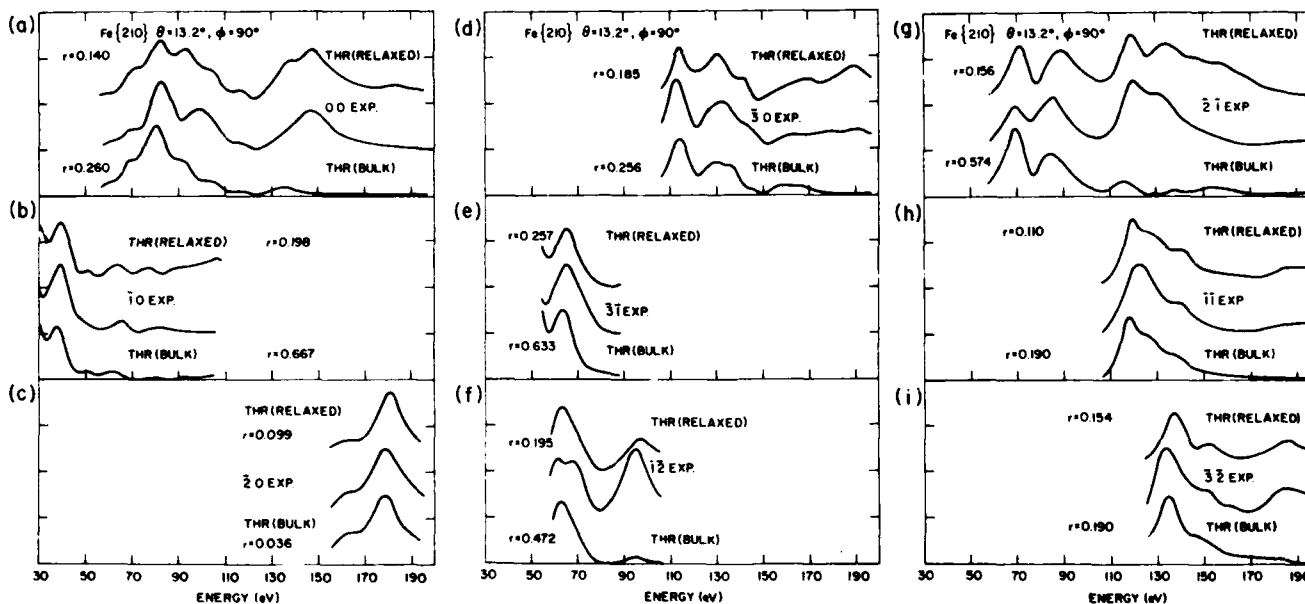


FIG. 6. Experimental and calculated LEED spectra for $\theta=0^\circ$. Theoretical curves are shown for both the bulklike and fully relaxed models.

FIG. 7. Same as for Fig. 6 but for $\theta=7.4^\circ$, $\phi=90^\circ$.FIG. 8. Same as for Fig. 6 but for $\theta=13.2^\circ$, $\phi=90^\circ$.

electronic structure of Na (a simple metal) and Fe (a transition metal) are important.

ACKNOWLEDGMENTS

Two of the authors (J.S. and F.J.) gratefully acknowledge partial support of this work by the Office of

Naval Research. J.S. also acknowledges financial support from the American Vacuum Society. The iron crystals used in this study were grown from ultrapure material provided by the American Iron and Steel Institute through Dr. C. A. Beiser of the National Steel Corporation and Dr. J. D. Myers of the Battelle Columbus Laboratories.

*Present address: Weizman Institute of Science, Rehovot, Israel.

¹H. L. Davis, J. R. Noonan, and L. H. Jenkins, Surf. Sci. 83, 559 (1979).

²D. L. Adams, H. B. Nielsen, J. N. Andersen, I. Stensgaard, R. Feidenhans'l, and J. E. Sorensen, Phys. Rev. Lett. 49, 669 (1982).

³H. B. Nielsen, J. N. Andersen, L. Petersen, and D. L. Adams, J. Phys. C 15, L1113 (1982).

⁴J. Sokolov, H. D. Shih, U. Bardi, F. Jona, and P. M. Marcus, J. Phys. C 17, 371 (1983).

⁵J. Sokolov, F. Jona, P. M. Marcus, Phys. Rev. B 29, 5402

(1984); Solid State Commun. 49, 307 (1984).

⁶M. W. Finnis and V. Heine, J. Phys. F 4, L37 (1974).

⁷R. N. Barnett, U. Landman, and C. L. Cleveland, Phys. Rev. Lett. 51, 1359 (1983).

⁸E. Zanazzi, F. Jona, D. W. Jepsen, and P. M. Marcus, Phys. Rev. B 14, 432 (1976).

⁹D. W. Jepsen, Phys. Rev. B 22, 5701 (1980).

¹⁰D. W. Jepsen, H. D. Shih, F. Jona, and P. M. Marcus, Phys. Rev. B 22, 814 (1980).

¹¹K. O. Legg, F. Jona, D. W. Jepsen, and P. M. Marcus, J. Phys. C 10, 937 (1977).

¹²E. Zanazzi and F. Jona, Surf. Sci. 62, 61 (1977).

Accession For

NTIS GRA&I	<input checked="" type="checkbox"/>
DTIC TAB	<input checked="" type="checkbox"/>
Unannounced	<input type="checkbox"/>
Justification	
By _____	
Distribution/	
Availability Codes	
Dist	Avail and/or Special
A-1	21 21

